Eur. Phys. J. B **4**, 413–420 (1998)

**THE EUROPEAN PHYSICAL JOURNAL B**



# The temperature dependence of the perpendicular giant magnetoresistance in Co/Cu multilayered nanowires

L. Piraux[1,a], S. Dubois[1], A. Fert[2], and L. Belliard[3]

[1] Unité de Physico-Chimie et de Physique des Matériaux, Université Catholique de Louvain, 1348 Louvain-la-Neuve, Belgium
[2] Unité Mixte de Recherche du Centre National de la Recherche Scientifique et de Thomson, Laboratoire Central de Recherches Thomson, 91404 Orsay, France
and
Université Paris-Sud, bâtiment 510, 91405 Orsay, France
[3] Laboratoire de Physique des Solides, Université Paris-Sud, 91405 Orsay, France

Received: 25 January 1998 / Accepted: 6 May 1998

**Abstract.** A theory, based on earlier work by Valet and Fert, is first presented to describe the influence of temperature on the perpendicular giant magnetoresistance (GMR) in multilayers. Then we present GMR measurements performed at $T = 77$ K and at room temperature on Co/Cu multilayered nanowires with layer thicknesses ranging from a few nm to 1 $\mu$m. We use our model to obtain a good quantitative fit to the experimental results in both the short spin diffusion length limit and out of this limit. We discuss the temperature dependence of the bulk parameters, the scattering spin asymmetry coefficient and spin diffusion length in the Co layers.

**PACS.** 72.15.Gd Galvanomagnetic and other magnetotransport effects – 75.70.-i Magnetic films and multilayers

## 1 Introduction

Since the pioneering work of Pratt *et al.* [1], measurements of the giant magnetoresistance (GMR) of magnetic multilayers in the CPP (current perpendicular to the planes) geometry have become increasingly attractive. Measurements have been performed on multilayers sandwiched between superconducting electrodes [1–4], microstructures fabricated by lithography methods [5], multilayers deposited on patterned substrates [6] and multilayered nanowires electrodeposited into cylindrical pores of track-etched polymer membranes [7–11].

A particular interest of the CPP-GMR arises from its dependence on the electron spin diffusion length (SDL) and, consequently, from its connection with other types of spin-injection effects [12,13]. However, the magnetoresistance does not depend on the SDL in the so-called long SDL limit, that is when the SDL is much larger than the individual layer thicknesses [12]. The SDL can be determined only when the individual layer thicknesses are larger than the SDL. As the SDL can approach the micron range in nonmagnetic metals, only few experiments have been performed in this regime with conventional multilayers. We can only refer to recent experiments performed on spin valve structures that allowed Steenwyck *et al.* to determine the SDL in permalloy [14], and also to experiments with nonmagnetic layers doped with paramagnetic impurities that shorten the SDL into the nanometer range [15]. In contrast, the nanowires offer a simple and convenient way to prepare multilayers with very thick layers. For Co/Cu, we have already reported measurements on sample series with layer thicknesses extending from a few nanometers up to 1 micron and we have determined the SDL of Co and Cu at low temperature [9,10]. In addition, unlike measurements performed on multilayers with superconducting contacts, measurements on multilayered nanowires can be performed at any temperature and used to determine the temperature dependence of the SDL.

In this article, we present extensive measurements of CPP-GMR on Co/Cu multilayers nanowires between low temperature and room temperature. This paper is organized as follows. In Section 2, we briefly report on the fabrication and characterization of arrays of multilayered nanowires and we describe the experimental procedure. In Section 3, we derive theoretical expressions of the CPP-GMR at finite temperature in the long SDL limit and out of this limit using an extension of the Valet-Fert (VF) model [12]. In Sections 4 and 5, we analyze our magnetoresistance data on Co/Cu multilayers obtained at low temperature and room temperature respectively. We focus particularly on the temperature dependence of the CPP-GMR, the influence of spin-mixing by electron-magnon scattering and the temperature dependence of the SDL.

[a] e-mail: piraux@pcpm.ucl.ac.be

Section 6 is devoted to supplementary discussions on the spin-relaxation processes. Finally, in Section 7, we present our conclusions.

## 2 Sample fabrication, characterization and experimental procedure

Track-etched polycarbonate membranes were used as nanoporous host material for the growth of multilayered nanowires [16]. A gold film serving as cathode was first evaporated on one side of the membrane. The membrane sample is then placed in a home-made Teflon cell and a 0.1 $cm^2$ area is exposed to the electrolyte. Electrodeposition is performed using an EG&G Princeton Applied Research Model 283 potentiostat/galvanostat under quiescent conditions at $T \sim 25°C$. Electrodeposited Co/Cu multilayered nanowires were made from a single bath using a pulsed deposition technique [7]. The Cu is kept in dilute concentration so that the rate of reduction of Cu is slow and limited by diffusion. The electrodeposition process is controlled by a computer which continuously integrates the charge during each layer deposition. The potential is switched when the deposition charges for the nonmagnetic and the magnetic layers reach the set value. Such a procedure is required to give uniform layer thicknesses all along the filament. The electrodeposition process is stopped when the wires emerge from the surface (as evidenced by a sudden increase of the plating current). The multilayer sample of about 90 nm in diameter shows an uniform cross section along the length of the filament. The microstructure of the multilayered nanowires was investigated in detail in reference [17] using X-ray diffraction and analytical transmission electron microscopy. The structure of the cobalt is hcp with a *c*-axis oriented almost perpendicular to the wire axis; the existence of a large number of stacking faults was also found.

Two series of Co/Cu multilayered nanowires were studied. In series 1, the Co layers have the shape of discs ($t_{Co} = 8$ or 25 nm) separated by Cu layers that can be very thick ($t_{Cu} = 10 - 150$ nm). In series 2, a typical sample is composed of Co rods ($t_{Co} = 60$ nm $- 1$ $\mu$m) separated by thin Cu layers ($t_{Cu} = 8$ nm $\ll$ diameter of the rods). The magnetic behavior of these two series of samples has already been discussed in recent papers [9,10]. For samples of series 1 (thin discs of Co separated by thick Cu layers), the plane perpendicular to the wire axis – that is the plane of the Co disc and also the plane of the *c*-axis of Co – is an easy plane. In contrast, for series 2, the axis of the wire is now an easy axis. Magnetoresistance measurements were performed at $T = 4.2$ K, 77 K and 300 K using the method described elsewhere [7]. We have also systematically performed the measurements in both field directions, parallel and perpendicular to the current, which allows us to correct the data for the small contribution from anisotropic magnetoresistance. Before presenting in Sections 4 and 5 the experimental results on the GMR, we present now our estimate of the resistivity of the copper layers that will be useful for the forthcoming analysis of the data. Such a determination was made using selected multilayer samples with Cu layers much thicker (by at least a factor 40) than the Co ones. In this case, the total measured resistance is almost completely due to copper. By measuring the resistance at $T = 77$ K and $T = 300$ K on several samples, we find that $\dfrac{\rho(300\text{ K})}{\rho(77\text{ K})}$ is always around 1.47. On the other hand, we know that $[\rho(300\text{ K}) - \rho(77\text{ K})]$ equals $1.45 \times 10^{-8}$ $\Omega$ m in pure copper so that we straightforwardly derive $\rho_{Cu}(300\text{ K}) = 4.55 \times 10^{-8}$ $\Omega$ m and $\rho_{Cu}(77\text{ K}) = 3.1 \times 10^{-8}$ $\Omega$ m.

## 3 Theoretical expressions of the CPP-GMR at finite temperature (influence of spin-mixing by electron-magnon scattering)

We begin by considering the classical long SDL limit with individual layer thicknesses much smaller than the SDL, *i.e.*

$$t_N \ll \ell_{sf}^{(N)}, \qquad t_F \ll \ell_{sf}^{(F)} \tag{1}$$

where $t_N(t_F)$ and $\ell_{sf}^{N}(\ell_{sf}^{(F)})$ are the thickness and SDL of the nonmagnetic (ferromagnetic) layers. In the long SDL limit and in the absence of spin-mixing [18] at temperatures much smaller than the Curie temperature, the VF model [12] predicts simple expressions of the CPP-GMR that are equivalent to those derived by a phenomenological resistor series model [2,3]. There are several ways of writing down these expressions and one of these is:

$$\left(\frac{\Delta R}{R^{AP}}\right)^{-\frac{1}{2}} = \left(\frac{R^{AP} - R^{P}}{R^{AP}}\right)^{-\frac{1}{2}} = \frac{\rho_F^* t_F + 2r_b^*}{\beta_0 \rho_F^* t_F + 2\gamma_0 r_b^*} + \frac{\rho_N^* t_N}{\beta_0 \rho_F^* t_F + 2\gamma_0 r_b^*} \tag{2}$$

where $\rho_F^*, \beta_0, \rho_N^*$ $r_b^*$ and $\gamma_0$ are defined by the following expressions of the resistivities and F/N interface resistances in the two channels ($\uparrow$ and $\downarrow$ refer to the majority and minority spin directions respectively)

$$\begin{aligned} \rho_{\uparrow(\downarrow)}^{F} &= 2\rho_F^*[1 - (+)\beta_0] \\ \rho_{\uparrow(\downarrow)}^{N} &= 2\rho_N^* \\ r_{\uparrow(\downarrow)} &= 2r_b^*[1 - (+)\gamma_0]. \end{aligned} \tag{3}$$

The notation $\beta(\gamma)$ is the usual one for the bulk (interface) scattering spin asymmetry coefficient and the index 0 in equations (2, 3) is to refer to the value of $\beta(\gamma)$ in the low temperature limit, that is when the inelastic scattering (phonons, magnons) is still much smaller than the elastic residual scattering (typically, this occurs below 100 K for usual values of the residual resistivity in multilayers). Although, in the initial VF model [12], expressions of the type of equation (2) had been derived in the simple case where $R^P$ and $R^{AP}$ are the resistances of parallel and antiparallel configurations, it can be shown [19] that the

resistance $R^{AP}$ is the same for a strict antiparallel arrangement and when, less drastically, $AP$ refers to a state with zero mean magnetization for a set of magnetic layers included within a total thickness range of the order of the SDL (the equivalence of antiparallel and random configurations has also been demonstrated in reference [20] in the simple case of infinite SDL).

In bulk ferromagnetic metals at finite temperature, the transfer of momentum between the spin ↑ and spin ↓ currents by spin flip electron-magnon scattering is expressed by introducing the spin mixing resistivity term $\rho_{\uparrow\downarrow}(T)$ in the transport equations [18]. In equation (2), spin mixing is ignored and equation (2) holds only in the temperature range where the spin-mixing resistivity term $\rho_{\uparrow\downarrow}$ is much smaller than $\rho_F^*$. If one takes into account typical values of $\rho_{\uparrow\downarrow}$ in ferromagnetic transition metals (roughly $10^{-12}\ T^2\ \Omega$ m [18]) and $\rho_F^*$ in multilayers (generally above $10^{-7}\ \ \Omega$ m), one finds that equation (2) can be used for the interpretation of our experimental results up to about 100 K, whereas spin mixing must be introduced for the interpretation at 300 K.

The spin mixing resistivity $\rho_{\downarrow\uparrow}(T)$ expressing the bulk electron-magnon scattering (inside the magnetic layers), has been introduced in the VF model by means of equation (38) of reference [19]. This result can be straightforwardly extended by introducing also an interface spin mixing resistance, $r_{\uparrow\downarrow}(T)$, that takes into account the contribution from the scattering by the spin fluctuations at the interfaces [21]. For a multilayer of unit area and M periods, one finds an equation quite similar to equation (38) of reference [19]

$$\sqrt{\Delta R\ R^{AP}} = \frac{M\left[\beta(T)\rho_F^*(T)t_F + 2\gamma(T)r_b^*(T)\right]}{1 + M\dfrac{\left[t_F\rho_{\uparrow\downarrow}(T) + 2r_{\uparrow\downarrow}(T)\right]}{R^{AP}}} \tag{4}$$

$$R^{AP} = M\left[\rho_F^*(T)t_F + \rho_N^*(T)t_N + 2r_b^*(T)\right]. \tag{5}$$

The parameters $\rho_F^*(T), \beta(T), \rho_N^*(T), r_b^*(T)$ and $\gamma(T)$ are defined from the spin ↑ and spin ↓ resistivities at temperature $T$ by:

$$\begin{aligned}
\rho^F_{\uparrow(\downarrow)}(T) &= 2\rho_F^*(T)[1 - (+)\beta(T)] \\
\rho^N_{\uparrow(\downarrow)}(T) &= 2\rho_N^*(T) \\
r_{\uparrow(\downarrow)}(T) &= 2r_b^*(T)[1 - (+)\gamma(T)]\cdot
\end{aligned} \tag{6}$$

As the spin dependence of the phonon and magnon contributions to the resistivity at temperature $T$ is generally different from the spin dependence of the residual resistivity, $\beta(T)$ and $\gamma(T)$ should generally be temperature dependent and different from $\beta_0$ and $\gamma_0$.

A straightforward transformation of equations (4, 5) leads to an expression similar to equation (2)

$$\left(\frac{\Delta R}{R^{AP}}\right)^{-\frac{1}{2}} = \frac{\rho^F_{eff}(T)t_F + 2r^b_{eff}(T)}{\beta_{eff}(T)\rho^F_{eff}(T)t_F + 2\gamma_{eff}(T)r^b_{eff}(T)} + \frac{\rho_N^*(T)t_N}{\beta_{eff}(T)\rho^F_{eff}(T)t_F + 2\gamma_{eff}(T)r^b_{eff}(T)} \tag{7}$$

where

$$\rho^F_{eff}(T) = \rho_F^*(T) + \rho_{\uparrow\downarrow}(T) \tag{8}$$

$$\beta_{eff}(T) = \frac{\beta(T)}{\left[1 + \dfrac{\rho_{\uparrow\downarrow}(T)}{\rho_F^*(T)}\right]} \tag{9}$$

$$r^b_{eff}(T) = r_b^*(T) + r_{\uparrow\downarrow}(T) \tag{10}$$

$$\gamma_{eff}(T) = \frac{\gamma(T)}{\left[1 + \dfrac{r_{\uparrow\downarrow}(T)}{r_b^*(T)}\right]}\cdot \tag{11}$$

Equation (7) has the same form as equation (2) and the influence of spin flip and non spin flip inelastic scattering is simply expressed by the replacement of $\beta_0, \rho_F^*, \gamma_0, r_b^*, \rho_N^*$ by $\beta_{eff}(T), \rho^F_{eff}(T), \gamma_{eff}(T), r^b_{eff}(T), \rho_N^*(T)$.

We next consider the theoretical predictions out of the long SDL limit and first at low temperature (*i.e.*, neglecting spin-mixing effects). In the limit where $t_F \gg \ell_{sf}^{(F)}$, with also $t_N \ll \ell_{sf}^{(N)}$ and $\rho_N^*\ t_N, r_b^* \ll \rho_F^*\ \ell_{sf}^{(F)}$, the general expressions of the VF model (Eqs. (40–42) in Ref. [12]), can be written as,

$$\frac{\Delta R}{R^P} = \frac{2\beta^2\ell_{sf}^{(F)}}{(1-\beta^2)t_F} \tag{12a}$$

where $\Delta R = R^{AP} - R^P$. Equation (12) strictly holds for the perfect antiparallel configuration schematically shown in Figure 1a. In the limit $t_F \gg \ell_{sf}^{(F)}$, $\Delta R$ is simply the sum of independent contributions from all the cells composed of a nonmagnetic layer sandwiched between two ferromagnetic layers of depth $\ell_{sf}^{(F)}$ (the shaded regions of Fig. 1a). However, the extension of equation (12) to other configurations is simple. When only a fraction $p$ of the pairs of ferromagnetic layers are antiparallel, only this fraction contributes to $\Delta R$, equation (12a) has to be multiplied by $p$ (for example, $p = 1/2$ for a random arrangement) and becomes

$$\frac{\Delta R}{R^P} = \frac{2p\beta^2\ell_{sf}^{(F)}}{(1-\beta^2)t_F}\cdot \tag{12b}$$

Alternatively, equation (12a) can be found directly by simple arguments. We first consider the antiparallel arrangement of Figure 1a. One knows from the theory of the CPP-GMR that spin ↑ and spin ↓ currents are approximately

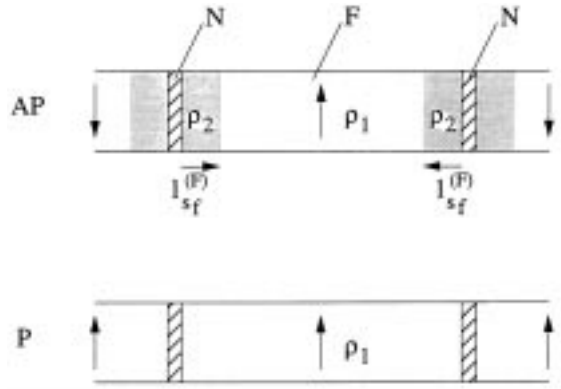


**Fig. 1.** Schematic representation of the parallel and antiparallel magnetic arrangement in multilayered nanowires in the short spin diffusion length limit; $\rho_1$ is the resistivity of the bulk ferromagnetic layer; $\rho_2$ denote the resistivity in the ferromagnetic layers within a distance $\ell_{sf}^{(F)}$ of the F/N interface for an antiparallel magnetic arrangement.

equal inside a depth $\ell_{sf}^{(F)}$ of the ferromagnetic material on both sides of the nonmagnetic layer. A reasonable approximation is to ascribe the resistivity $\rho_2 = \rho_F^* = \dfrac{\rho_\uparrow^F + \rho_\downarrow^F}{4}$ to this depth and the resistivity of the bulk ferromagnetic material, $\rho_1 = \rho_F^*(1-\beta^2) = \dfrac{\rho_\uparrow^F \rho_\downarrow^F}{(\rho_\uparrow^F + \rho_\downarrow^F)}$, to the inner part of the ferromagnetic layer. When we also neglect the resistance of the nonmagnetic layer and the interface resistance (since we suppose $\rho_F^* \ell_{sf}^{(F)} \gg \rho_N^*\ t_N, r_b^*$), this gives for the resistance of one period

$$R^{AP} = 2\rho_F^* \ell_{sf}^{(F)} + \rho_F^*(1-\beta^2)\Big(t_F - 2\,\ell_{sf}^{(F)}\Big). \qquad (13)$$

For a parallel arrangement (Fig. 1b), the resistivity is approximately that of the bulk ferromagnetic material everywhere, *i.e.*, for one period

$$R^P = \rho_F^*(1-\beta^2)t_F \qquad (14)$$

and calculating $\Delta R/R^P$ leads exactly to equation (12a) derived from the general equation of the VF model.

At finite temperature, spin mixing due to electron-magnon scattering tends to equalize the spin $\uparrow$ and spin $\downarrow$ currents in the magnetic layers. On the scheme of Figure 1a for an antiferromagnetic configuration, the resistivity inside a depth $\ell_{sf}^{(F)}$ on either side of the nonmagnetic layer is still $\rho_2 = \rho_F^*$. The resistivity in the inner part of the ferromagnetic layer is the resistivity $\rho_1$ of the bulk ferromagnet at temperature $T$. Using the canonical expression of the two current model [18], we obtain

$$\rho_1 = \frac{\rho_\uparrow^F(T)\rho_\downarrow^F(T) + \rho_{\uparrow\downarrow}(T)(\rho_\uparrow^F(T) + \rho_\downarrow^F(T))}{\rho_\uparrow^F(T) + \rho_\downarrow^F(T) + 4\ \rho_{\uparrow\downarrow}(T)}$$
$$= \rho_F^*(T)\frac{(1-\beta(T)^2)\rho_F^*(T) + \rho_{\uparrow\downarrow}(T)}{\rho_F^*(T) + \rho_{\uparrow\downarrow}(T)}\,. \qquad (15)$$

In the ferromagnetic configuration, the resistivity is $\rho_1$ elsewhere and, consequently, we get

$$\Delta R = 2\rho_F^*(T)\ell_{sf}^{(F)}\left[1 - \frac{(1-\beta(T)^2)\rho_F^*(T) + \rho_{\uparrow\downarrow}(T)}{\rho_F^*(T) + \rho_{\uparrow\downarrow}(T)}\right] \qquad (16)$$

and

$$R^P = \rho_F^*(T)t_F\frac{(1-\beta^2(T))\rho_F^*(T) + \rho_{\uparrow\downarrow}(T)}{\rho_F^*(T) + \rho_{\uparrow\downarrow}(T)}, \qquad (17)$$

so, finally

$$\frac{\Delta R}{R^P} = \frac{2\beta(T)^2}{(1-\beta(T)^2) + \dfrac{\rho_{\uparrow\downarrow}(T)}{\rho_F^*(T)}}\frac{\ell_{sf}^{(F)}}{t_F}$$
$$= \frac{2\beta_{eff}^2(T)}{\left(\dfrac{\rho_F^*(T)}{\rho_{eff}^F(T)} - \beta_{eff}^2(T)\right)}\frac{\ell_{sf}^{(F)}}{t_F}. \qquad (18)$$

Here again, $\Delta R$ is expected to be multiplied by $p$ when the proportion of antiparallel orientations of the magnetization in consecutive layers is $p$.

## 4 GMR in the low temperature limit

The low temperature limit described by equations (2, 12) corresponds to the regime where the spin mixing resistivity $\rho_{\uparrow\downarrow}$ and the inelastic contributions to $\rho_\uparrow$ and $\rho_\downarrow$ are still much smaller than the residual values of $\rho_\uparrow$ and $\rho_\downarrow$. In Section 3, we have estimated that this regime extends to about 100 K for our samples. This is confirmed by the negligible (a few %) variation of the resistance and magnetoresistance between 4.2 K and 77 K. Here we present only the more extensive data obtained at 77 K.

In Figure 2, we show a plot of $\left(\dfrac{\Delta R}{R^{AP}}\right)^{-1/2}$ at 77 K *vs.* the thickness of Cu, for samples of series 1 with $t_{\mathrm{Co}} = 8$ nm and 25 nm. For $t_{\mathrm{Cu}}$ smaller than about 100-150 nm, we observe two linear variations, as expected from equation (2) for the long SDL limit (for $t_{\mathrm{Cu}} \geq 100$ nm, the magnetization of consecutive discs can only be randomly oriented in the plane of the discs at the coercive field and equation (2) holds; the continuation of the linear variation down to 10 nm indicates that the condition of zero magnetization over the SDL remains fulfilled throughout the series). Equation (2) also predicts that the straight lines for different values of $t_{\mathrm{Co}}$ cross at a point having $t_{\mathrm{Cu}}^* = \dfrac{2(\gamma_0 - \beta_0)r_{\mathrm{Co/Cu}}^*}{\beta_0\rho_{\mathrm{Cu}}^*}$ and $\beta_0^{-1}$ for coordinates. The crossing of the two straight lines of Figure 2 at a positive value of $t_{\mathrm{Cu}}$ indicates that $\gamma_0$ is larger than $\beta_0$. On the other hand, the vertical coordinate of the crossing point allows us a direct determination of $\beta_0$:

$$\beta_0 \sim 0.36 \pm 0.02.$$

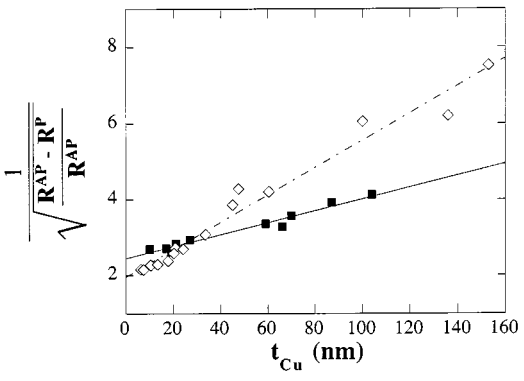


**Fig. 2.** Plot of $\frac{1}{\sqrt{\frac{R^{AP}-R^{P}}{R^{AP}}}}$ *vs.* $t_{\mathrm{Cu}}$ for Co/Cu multilayered nanowires for two different Co layer thicknesses $t_{\mathrm{Co}}$ (lozenges: 8 nm, squares: 25 nm) at $T = 77$ K.

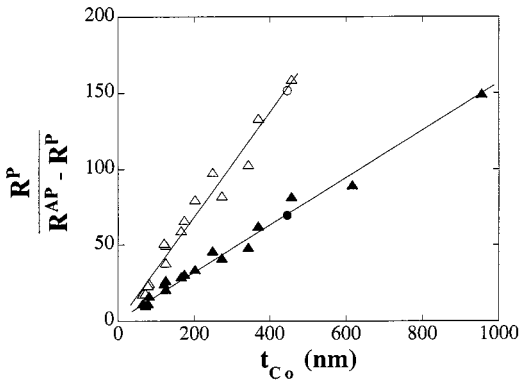


**Fig. 3.** Linear variation of the inverse magnetoresistance *vs.* $t_{\mathrm{Co}}$ for Co ($t_{\mathrm{Co}}$)/Cu (8 nm) multilayered nanowires at $T = 77$ K (filled symbols) and $T = 300$ K (open symbols). The circles refer to data obtained on a Co (435 nm)/Cu (15 nm) sample.

The determination of the other parameters involved in equation (2) was made by identifying the equations of the straight lines in Figure 2 with equation (2) and has been explicitly described in reference [10]. We obtain: $\rho^{*}_{\mathrm{Co}} \sim 18 \pm 2\times10^{-8}\ \Omega$ m, $\beta_0 \sim 0.36 \pm 0.02$, $r^{*}_{\mathrm{Co/Cu}} \sim 3 \pm 1.5\times10^{-16}\ \Omega\ \mathrm{m}^2$ and $\gamma_0 \sim 0.85 \pm 0.15$ ($\rho^{*}_{\mathrm{Cu}} \sim 3\times10^{-8}\ \Omega$ m is determined in Sect. 2). We note that, in our Co/Cu multilayers, the interface scattering is more strongly spin dependent than the bulk one. However, the proportion of the respective contributions from bulk and interface scattering depends on the Co thickness. For a more quantitative comparison of these respective contributions, it can be shown straightforwardly that the bulk contribution to $\left(\frac{\Delta R}{R^{AP}}\right)^{1/2}$, proportional to $\beta_0\rho^{*}_{\mathrm{Co}}t^{*}_{\mathrm{Co}}$, exceeds the interface contribution, proportional to $2\gamma_0 r^{*}_{\mathrm{Co/Cu}}$, for $t_{\mathrm{Co}}$ larger than about 7.5 nm. As a consequence, in the samples of series 1 (with $t_{\mathrm{Co}} = 8$ nm and 25 nm), the major contributions comes from the the bulk scattering, which explain the larger uncertainties in the determination of the interface parameters.

In Figure 3, a plot showing $\frac{R^P}{\Delta R}$ at 77 K *vs.* $t_{\mathrm{Co}}$ is shown for samples of series 2 with $t_{\mathrm{Cu}} = 8$ nm and $t_{\mathrm{Co}}$ varying between 60 and 950 nm. The data obtained on a sample with $t_{\mathrm{Cu}} = 15$ nm and $t_{\mathrm{Co}} = 435$ nm are also reported on the same plot (see the caption). As expected from equation (12b), the GMR does not depend on the thickness of the Cu layers seeing that $\rho^{*}_{\mathrm{Cu}}t_{\mathrm{Cu}} \ll \rho^{*}_{\mathrm{Co}}l^{(\mathrm{Co})}_{sf}$. We observe the linear variation expected from equation (12b) when the proportion $p$ of antiparallel pairs of consecutive Co layers is constant throughout the series. In a previous publication [10], we have described the magnetic behavior of the Co/Cu nanowires and proposed that, at the coercive field, the nanowires present an approximately random magnetic arrangement of consecutive Co layers. This is confirmed by our recent MFM measurement. An example of MFM data and its interpretation is shown in Figure 4 for a (Co 170 nm/Cu 8 nm) nanowire. The magnetization is parallel to the axis of the wire (note the pole at the end of the wire on the left, in white on the image) and arrows represent its orientation in successive cobalt layers. The dashed lines represent copper layers and two arrows converging (diverging from) a copper layer account for the corresponding maximum (minimum) of the MFM signal profile. On the other hand, when the magnetizations on both sides of the very thin copper layers are parallel (longer arrows), the MFM signal is approximately flat at an intermediate level and the image above is grey. Antiferromagnetic (AF) ranges, in which the magnetic period is clearly twice the chemical period, alternate with ferromagnetic (F) ranges (approximately flat signal) and ranges with a more random distribution of F and AF arrangements. The final balance is 39% of pairs of consecutive Co layers having antiparallel magnetizations. This is at $H = 0$ and not at the field $\pm H_c$ of the MR peaks. Moreover, we know that $\Delta R/R^P$ of our samples increases by a factor of about 1.25 between zero field and the peak. As $\Delta R/R^P$ is expected to be proportional to $p$ in the thickness range where equation (12b) holds, we can estimate that $p$ is about 0.49 at the MR peak.

We have found similar values of $p$, ranging from 0.33 and 0.49 for several nanowires of the same series (Co 170 nm/Cu 8 nm). In addition, according to equation (12b), the linear variation of $\Delta R/R^P$ displayed in Figure 3 indicates that $p$ does not changes significantly throughout series 2. Consequently, for all samples of series 2, we have assumed

$$0.33 < p < 0.49.$$

When these values of $p$ and $\beta_0 \sim 0.36 \pm 0.02$ are introduced into equation (12b), the interpretation of the slope of Figure 3 leads to

$$l^{(\mathrm{Co})}_{sf} \sim 59 \pm 18\ \mathrm{nm}.$$

The uncertainty on the value of $l^{(\mathrm{Co})}_{sf}$ is primarily due to the uncertainty on $p$. Extensive MFM measurements on a large number of nanowires – for a better statistics – should allow us to reduce this uncertainty.

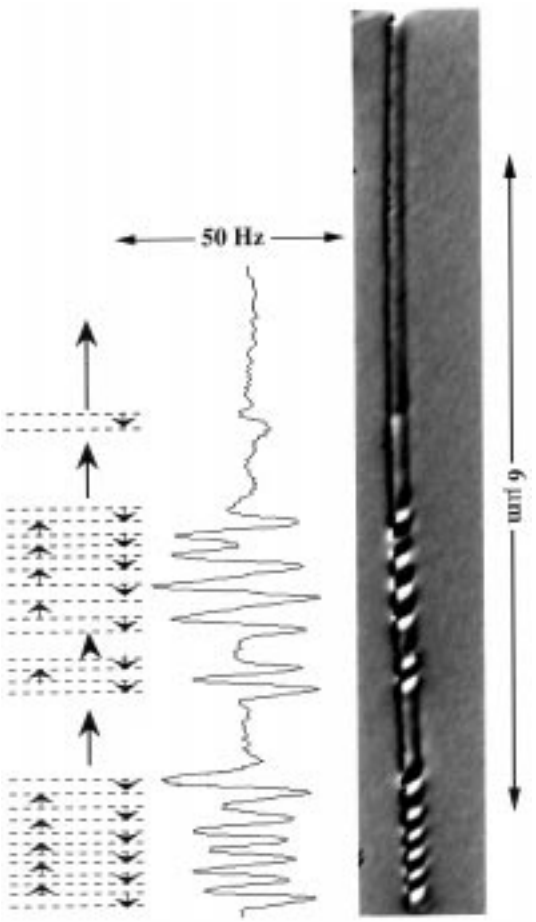


**Fig. 4.** Above: MFM image of a Co (170 nm)/Cu (8 nm) nanowire at zero field. The right end of the wire is outside the image. Middle: profile of the MFM signal along the wire. Below : interpretation of the MFM data above. The dashed lines represent copper layers (only 8 nm thick) and arrows represent the direction of the magnetization in the thick cobalt. Arrows converging towards (diverging from) a Cu layer are associated with maxima (minima) of the profile and white (black) in the image. Ranges with an approximate flat profile at an intermediate level (grey on the image) are identified with parts of the sample with parallel magnetizations in consecutive cobalt layers (we have not drawn dashed lines and individual arrows in these ranges). The proportion of antiferromagnetic ordering of consecutive Co layers is 39% in the sample of the figure.

## 5 Influence of temperature on the GMR and the spin diffusion length

In Figure 5, we show the variation of $\left(\frac{\Delta R}{R^{AP}}\right)^{-\frac{1}{2}}$ at room temperature (RT) as a function of $t_{\rm Cu}$ for samples of series 1 with $t_{\rm Co} = 8$ nm and 25 nm. As expected from equation (7), two straight lines fit the experimental data. In principle, from equation (7), the 4 unknown parameters, $\rho_{eff}^{\rm Co}$, $\beta_{eff}$, $r_{eff}^{\rm Co/Cu}$ and $\gamma_{eff}$ can be determined from the equations of the two straight lines. However, we prefer the less global but more transparent following analysis.

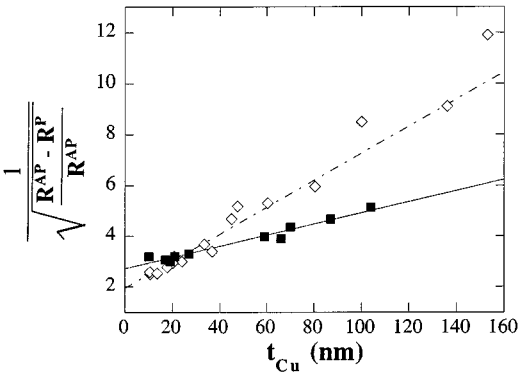


**Fig. 5.** Plot of $\frac{1}{\sqrt{\frac{R^{AP}-R^{P}}{R^{AP}}}}$ *vs.* $t_{\rm Cu}$ for Co/Cu multilayered nanowires for two different Co layer thicknesses $t_{\rm Co}$ (lozenges: 8 nm, squares: 25 nm) at $T = 300$ K.

First, $\beta_{eff}(300\ {\rm K})$ can be directly and unambiguously determined from the vertical coordinate of the crossing point of the two straight lines in Figure 5. We get:

$$\beta_{eff}(300\ {\rm K}) = 0.31 \pm 0.02.$$

$\beta_{eff}(300\ {\rm K})$ is smaller than $\beta_0$ and, according to equation (9), this reduction can have two origins: smaller value of $\beta(300\ {\rm K})$ compared to $\beta_0$ and/or influence of the factor $\left[1 + \frac{\rho_{\uparrow\downarrow}(T)}{\rho^*_{\rm Co}(T)}\right]^{-1}$. The factor $\left[1 + \frac{\rho_{\uparrow\downarrow}({\rm T})}{\rho^*_{\rm Co}({\rm T})}\right]^{-1}$ can be calculated approximately: $\rho^*_{\rm Co}(300\ {\rm K})$ can be estimated at 25 $\mu\Omega$ cm by adding the room temperature resistivity of pure cobalt (7 $\mu\Omega$ cm) to the residual value of $\rho^*_{\rm Co}$ ($\sim$ 18 $\mu\Omega$ cm) obtained in Section 4; on the other hand, by extrapolating published values of $\rho_{\uparrow\downarrow}$ for Co [24] to RT, we find $\rho_{\uparrow\downarrow}(300\ {\rm K}) \sim 4\ \mu\Omega$ cm. By introducing the above values of $\rho^*_{\rm Co}(300\ {\rm K})$ and $\rho_{\uparrow\downarrow}(300\ {\rm K})$ into equation (7), we find $\beta(300\ {\rm K}) \sim 0.36$. We thus obtain the same value (approximately) for $\beta$ at low temperature and RT, the factor $\left[1 + \frac{\rho_{\uparrow\downarrow}({\rm T})}{\rho^*_{\rm Co}({\rm T})}\right]^{-1}$ being sufficient to account for the smaller value of $\beta_{eff}(300\ {\rm K})$. It is not surprising to find that $\beta(300\ {\rm K})$ is as large as $\beta_0$, since the experiments on bulk Co alloys [24] have already shown that the inelastic scattering (phonons) is fairly spin dependent in cobalt (it can be pointed out that, even if one assumes $\rho_{\uparrow\downarrow}(300\ {\rm K}) = 0$, one gets $\beta(300\ {\rm K}) = 0.31$, which is not much smaller than $\beta_0 = 0.36$). Besides $\beta_{eff}(300\ {\rm K})$, the parameter that can be determined the most accurately is the SDL, $\ell_{sf}^{({\rm Co})}(300\ {\rm K})$. In Figure 3, we show a plot of $R^P/\Delta R$ at RT *vs.* $t_{\rm Co}$ for samples of series 2. As at low temperature, we observe a linear variation (in agreement with Eq. (18)), but the slope at RT is approximately twice that at 77 K. It can be seen straightforwardly that this increase of the slope is primarily due to some shortening of $\ell_{sf}^{({\rm Co})}$ at RT. By introducing into equation (18) $\beta_{eff}(300\ {\rm K}) \sim 0.31$ and $\rho_{eff}^{\rm Co} = \rho^*_{\rm Co}(300\ {\rm K}) + \rho_{\uparrow\downarrow}(300\ {\rm K}) \sim 29\ \mu\Omega$ cm and supposing, as in Section 3, $0.33 < p < 0.49$, we account for the

slope of Figure 5 with

$$\ell_{sf}^{(\mathrm{Co})}(300\ \mathrm{K}) \sim 38 \pm 12\ \mathrm{nm}.$$

As at low temperature, the uncertainty on $\ell_{sf}^{(\mathrm{Co})}$ is primarily due to the uncertainty on $p$.

The value of $r_{eff}^{\mathrm{Co/Cu}}(300\ \mathrm{K})$ and $\gamma_{eff}(300\ \mathrm{K})$ derived by fitting the straight lines of Figure 4 with equation (7) differ from the values at low temperature by less than the error bar of their determination, which makes no sense for a discussion of the temperature dependence of the interface parameters.

## 6 Discussion on the spin-relaxation processes

The most important experimental result of this work is the determination of the spin diffusion length in a ferromagnetic metal (Co) and of its temperature dependence. In the low temperature limit, the SDL in Co ($\ell_{sf}^{(\mathrm{Co})} \sim 59$ nm) is definitely shorter than the SDL in Cu ($\ell_{sf}^{(\mathrm{Cu})} \sim 150$ nm, see Ref. [10]). This shorter value in Co compared to Cu is consistent with the faster spin-orbit scattering rate expected from the strong $d$ character of the carriers in Co ($s$-$d$ and $d$ states) [25]. The SDL decreases from 59 nm in the low temperature limit to 38 nm at RT, which is a moderate decrease and account for the moderate reduction of the GMR at RT. We recall that the SDL is related to the spin-lattice relaxation rate [12,19]. It has been argued in Section 5.2 of reference [19] that this relaxation is due to the spin-orbit scattering and that the spin-flip scattering by magnons is not a direct spin-lattice relaxation mechanism. This argument is confirmed by the moderate reduction of the SDL at RT. If the electron-magnon scattering was a spin-lattice relaxation mechanism, the SDL at RT would be much shorter than we find in our experiments. In a simple free electron model, for example, the relaxation rate $\tau_{\uparrow\downarrow}^{-1}$ derived from $\tau_{\uparrow\downarrow}^{-1} = ne^2\rho_{\uparrow\downarrow}/m$ with $\rho_{\uparrow\downarrow}(RT) \sim 4\ \mu\Omega$ cm and an electron density per spin direction, $n$, corresponding to 0.5 electron per atom, is $\tau_{\uparrow\downarrow}^{-1} \sim 5\times10^{13}\ \mathrm{s}^{-1}$ which gives $\lambda_{\uparrow\downarrow} \sim 31.5$ nm for the spin mean free path. The corresponding SDL [12]

$$\ell_{sf}^{(\mathrm{Co})} = \left(\frac{\lambda_{\mathrm{Co}}^{*}\lambda_{\uparrow\downarrow}}{6}\right)^{1/2}$$

with $\lambda_{\mathrm{Co}}^{*} = \left(\frac{1}{\lambda_{\uparrow}} + \frac{1}{\lambda_{\downarrow}}\right)^{-1} = mv_F/2ne^2\rho_{\mathrm{Co}}^{*}$ would be as short as 3.65 nm, about 10 times shorter than the experimental SDL at RT. According to the discussion of reference [19], electron-magnon collisions can only transfer spin accumulation between the s and d bands (equalization of the out of equilibrium magnetization within the electron system) and the spin-lattice relaxation rate is governed only by the spin-orbit scattering on defects, impurities and phonons. The reduction of the SDL from 59 nm to 38 nm at RT can be ascribed to the spin relaxation by the spin-orbit part of the scattering by phonons, to the reduction of the mean free path and, partly, to some influence of the equalization of the spin accumulation within the electron system on the spin-orbit relaxation rate.

To sum up the question of the spin relaxations, we can say:

i) The spin-mixing relaxation rate $\tau_{\uparrow\downarrow}^{-1}$ (involved in $\rho_{\uparrow\downarrow}$ and characteristic of the momentum transfer between the spin $\uparrow$ and spin $\downarrow$ electrons) is essentially due to spin-flip scattering by magnons [18]. The contribution from spin-orbit scattering, estimated from our results on the SDL of Co, contributes negligibly to $\rho_{\uparrow\downarrow}$ (in the same free electron model as above, $\ell_{sf}^{(\mathrm{Co})} \sim 38$ nm corresponds to $\tau_{sf}^{-1} \sim 4.6\times10^{11}\ \mathrm{s}^{-1}$ for the spin-orbit relaxation rate to be compared to $\tau_{\downarrow\uparrow}^{-1} \sim 5\times10^{13}\ \mathrm{s}^{-1}$ for the electron-magnon relaxation rate involved in the RT value of $\rho_{\uparrow\downarrow}$).

ii) The spin-lattice relaxation rate $\tau_{sf}^{-1}$ (involved in the SDL) depends moderately on temperature ($2.6\times10^{11}\ \mathrm{s}^{-1}$ at 77 K, $4.6\times10^{11}\ \mathrm{s}^{-1}$ at 300 K). This spin-lattice relaxation is essentially due to spin-orbit scattering, at low temperature (spin-orbit part of the elastic scattering by defects or impurities) as well as at RT (with some additional contribution from the spin-orbit part of inelastic scattering). The spin-flip scattering by magnons is not a spin-lattice relaxation process.

iii) The SDL in Co is relatively short (59-38 nm), much shorter than in noble metals [10] but definitely larger than in permalloy ($\sim 5$ nm [14,26]). It can be pointed out that the short SDL of ferromagnetic metals and alloys reduces the output voltage [27] expected for spin injection devices such as the spin transistor introduced by Johnson [13].

## 7 Conclusions

We have proposed an extension of the earlier model by Valet and Fert for the perpendicular giant magnetoresistance in multilayers at finite temperature taking into account spin-mixing of the spin $\uparrow$ and spin $\downarrow$ currents and the effect of phonons. Simple expressions were derived in both the long SDL limit and the short SDL limit. Next, we have presented and analyzed the first experiments of CPP-GMR at room temperature in Co/Cu multilayered nanowires. We find that the spin diffusion length in cobalt is relatively short ($\sim 59$ nm at low temperature), much shorter than in noble metals, and does not depend much on temperature ($\sim 38$ nm at RT). We have also determined the scattering spin asymmetry coefficient; the interface asymmetry is definitely larger than the bulk one ($\gamma \sim 0.85$ compared to $\beta \sim 0.36$ at low temperature), and the crossover from interface-dominated to bulk-dominated GMR occurs around $t_{\mathrm{Co}} = 8$ nm.

We thank Whatman s.a. (Belgium) for providing the polycarbonate membrane samples used in this study. L.P. is a Research Associate of the National Fund for Scientific Research

(Belgium). This work has been partly supported by a Brite programme of the European Commission (BE95-1761) and by the Belgian Interuniversity Attraction Pole Program (PAI-IUAP P4/10).

## References


1. W.P. Pratt, S.F. Lee, J.M. Slaughter, R. Loloee, P.A. Schroeder, J. Bass, Phys. Rev. Lett. **66**, 3060 (1991).
2. S.F. Lee, W.P. Pratt, R. Loloee, P.A. Schroeder, J. Bass, Phys. Rev. B **46**, 548 (1992).
3. W.P. Pratt, S.F. Lee, P. Holody, Q. Yang, R. Loloee, J. Bass, P.A. Schroeder, J. Magn. Magn. Mater. **126**, 406 (1993)
4. N.J. List, W.P. Pratt, M.A. Howson, J. Xu, M.J. Walker, D. Greig, J. Magn. Magn. Mater. **148**, 342 (1995).
5. M.A. Gijs, S.K.J. Lenczowski, J.B. Giesbers, Phys. Rev. Lett. **70**, 3343 (1993); W. Vavra, S.F. Cheng, A. Fink, J.J. Krebs, G.A. Prinz, Appl. Phys. Lett. **66**, 2579 (1995).
6. M.A. Gijs, M.T. Johnson, A. Reinders, P.E. Huijsman, R.J.M. van de Veerdonk, S.K.J. Lenczowski, R.J.M. Gansewinkel, Appl. Phys. Lett. **66**, 1839 (1995); T. Ono, T. Shinjo, J. Phys. Soc. Jpn **64**, 363 (1995).
7. L. Piraux, J.M. George, J.F. Despres, C. Leroy, E. Ferain, R. Legras, K.Ounadjela, A. Fert, Appl. Phys. Lett. **65**, 2484 (1994).
8. B. Voegeli, A. Blondel, B. Doudin, J.Ph. Ansermet, J. Magn. Magn. Mater. **151**, 388 (1995).
9. L. Piraux, S. Dubois, C. Marchal, J.M. Beuken, L. Filipozzi, J.F. Despres, K. Ounadjela, A. Fert, J. Magn. Magn. Mater. **156**, 317 (1996).
10. L. Piraux, S. Dubois, A. Fert, J. Magn. Magn. Mater. **159**, L287-L292 (1996).
11. S. Dubois, C. Marchal, J.M. Beuken, L. Piraux, J.L. Duvail, A. Fert, J.M. George, J.L. Maurice, Appl. Phys. Lett. **70**, 396 (1997).
12. T. Valet, A. Fert, Phys. Rev. B **48**, 7099 (1993).
13. M. Johnson, Phys. Rev. Lett. **70**, 2142 (1993).
14. Steenwyck *et al.*, J. Magn. Magn. Mater. **170**, L1 (1997).
15. Q. Yang, P. Holody, S.F. Lee, L.L. Henry, R. Loloee, P.A. Schroeder, W.P. Pratt Jr., J. Bass, Phys. Rev. Lett. **72**, 3274 (1994).
16. E. Ferain R. Legras, Nucl. Instrum. Meth. B **82**, 539 (1993); E. Ferain R. Legras, Nucl. Instrum. Meth. B **84**, 331 (1994).
17. J. L. Maurice, D. Imhoff, P. Etienne, O. Durand, S. Dubois, L. Piraux, J.M. George, P. Galtier, A. Fert, J. Magn. Magn. Mater. **184**, 1 (1998).
18. A. Fert, I.A. Campbell, J. Phys. F **6**, 849 (1976).
19. A. Fert, J.L. Duvail, T. Valet , Phys. Rev. B **52**, 6513 (1995).
20. S. Zhang, P.M. Levy, Phys. Rev. B **47**, 6776 (1993).
21. T Ono, Y. Sugita, K. Shigeto, K. Mibu, N. Hosoito, T. Shinjo, Phys. Rev. B **55**, 14457 (1997).
22. L. Piraux, S. Dubois, E. Ferain, R. Legras, K. Ounadjela, J.M. George, J.L. Maurice, A. Fert, J. Magn. Magn. Mater. **165**, 352 (1997).
23. L. Belliard *et al.* (to be published).
24. B. Loegel, F. Gautier, J. Phys. Chem. Solids **32**, 2723 (1971).
25. F. Beuneu, P. Monod, Phys. Rev. B **13**, 3424 (1976); P. Monod, S. Schultz, J. Phys. France **43**, 393 (1982).
26. S. Dubois *et al.* (to be published).
27. A. Fert, S.F. Lee, Phys. Rev. B **53**, 6554 (1996).